Hindawi Publishing Corporation
International Journal of Antennas and Propagation
Volume 2015, Article ID 595023, 10 pages
http://dx.doi.org/10.1155/2015/595023

Research Article

Numerical and Experimental Verification of a 3D Quasi-Optical System

Zejian Lu,[1] Xiaoming Liu,[1] Hai Wang,[1] Xiaodong Chen,[2] Yuan Yao,[1] and Junsheng Yu[1]

[1]*School of Electronic Engineering, Beijing University of Posts and Telecommunications, Beijing 100876, China*
[2]*School of Electric Engineering and Computer Science, Queen Mary University of London, London E1 4NS, UK*

Correspondence should be addressed to Zejian Lu; lzj_bupt@bupt.edu.cn

Received 26 January 2015; Revised 9 May 2015; Accepted 10 May 2015

Academic Editor: Atsushi Mase

A modular and efficient Gaussian beam (GB) analysis method, incorporating frame-based Gabor transformation, GB reflection, and a 3D GB diffraction technique, was developed to analyze both the reflectors and frequency selective surface (FSS) in quasi-optical (QO) system. To validate this analysis method, a 3D dual-channel QO system operating at 183 and 325 GHz was designed and tested. The proposed QO system employs two-layer structure with a FSS of perforated hexagonal array transmitting the 325 GHz signal on the top layer while diverting the 183 GHz signal to the bottom layer. Measured results of the system demonstrate that the agreement can be achieved down to −30 dB signal level for both channels in the far field pattern. The discrepancy between the calculation and measurement is within 2 dB in the main beam region (2.5 times −3 dB beamwidth), verifying the effectiveness and accuracy of the proposed method.

1. Introduction

Quasi-optical network (QON) system normally consists of several feed horns and cascaded mirrors or other signal-conditioning components. A QON transmits electromagnetic waves in free space, bearing advantages of multichannel, multipolarization with low path loss and good compatibility. Due to these benefits, QON is widely utilized in millimeter and submillimeter wave remote sensing and radioastronomy applications [1]. Many missions have been or are being developed, such as the five frequencies' band MASTER limb sounding instrument [2], the three bands' MARSCHALS simulator [3], the Herschel and Planck space telescopes [4–6], the ALMA front-end system [7, 8], and the underway Chinese FY-4 meteorological satellite whose working frequencies are 54, 118, 183, 380, and 425 GHz [9].

There are two trends for the development of QON systems. One is that more and more channels are to be squeezed into a single instrument, imposing a big challenge to the design process. Unfortunately, most of the current designs are in a 2D configuration, where the optical centers of the elements are all in the same plane. In a payload of limited space, a 3D QON can significantly increase the compactness. The other trend is that the operating frequency goes up to the terahertz band, where the dimension of the elements is in the order of hundreds and even thousands of wavelengths. For these electrically large systems, Physical Optics (PO) method produces very accurate prediction on the electrical performance of a QON system, while suffering from heavy computational cost. In comparison, Geometrical Optics (GO) method is not capable of analyzing caustic region where all the rays converge together. Therefore, efficient and accurate algorithms are required for the analysis of electrically large 3D QON. Besides this, an increasing number of quasi-optical components, such as frequency selective surfaces (FSSs) and polarizing grids, are integrated into a QON system, demanding that the algorithm must be highly modular and able to interface with other computational methods. A fast method, namely, diffracted Gaussian beam analysis (DGBA), was developed to analyze QON system by taking the edge diffraction into account [10]. The modular nature of this method makes it easily interface with Periodic

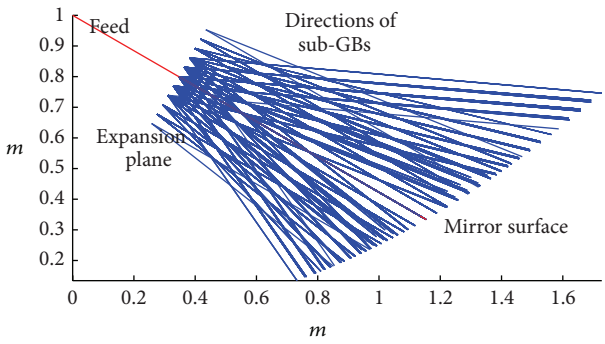

Figure 1: Scheme of frame-based Gabor transformation.

Method of Moment (PMM), which is used to analyze FSSs. The DGBA and PMM methods are later integrated together in a visual design program to analyze QON system [11]. However, this method cannot be regarded as a rigorous 3D diffraction solution due to its 2D modeling nature. Recently, another modular Gaussian beam analysis method based on 3D diffraction technique is proposed in [12] and this method can also be integrated with FSS analysis in the same manner of DGBA.

In this paper, a dual-channel 3D QON system is designed, fabricated, and tested. The two channels are the atmospheric sounding frequencies at 183 GHz and 325 GHz, both working at water vapor absorption line. This QON system can serve as a prototype of 3D structure for a Chinese meteorological satellite radiometer.

The rest of the paper is organized as follows: Section 2 gives a brief introduction to the modular Gaussian beam analysis method based on 3D diffraction technique integrated with FSS simulation; Section 3 presents the design of the QON system and the key components; the experimental validation of the proposed GB analysis method is shown in Section 4.

2. Gaussian Beam Analysis Method

A modular Gaussian beam analysis method based on 3D diffraction technique has been proposed in [12] to analyze the reflector-based antenna systems, which consists of frame-based Gabor transformation, GB reflection, and a 3D GB diffraction technique developed to handle the scattering from the reflector edge. In the analysis of reflectors, the field radiated from the feed horn or previous reflector can be expanded into a set of sub-GBs via frame-based Gabor transformation and then these individual GBs are traced into the reflector where reflection or diffraction occurs. The total radiation field, either near field or far field, can be evaluated by the summation of all the sub-GBs.

Figure 1 illustrates the frame-based Gabor transformation in the analysis of an offset reflector. The expansion plane is chosen at a certain distance away from the feed horn and the tangential field E_x on the plane can be represented by summation of sub-GBs, as defined in the following [10]:

$$E_x(x,y,z) = \sum_{m,n,\mu,\nu} \exp\left[j\left(mn+\mu\nu\right)K_0L_0\right] \cdot A^x_{m,n,\mu,\nu} B_{m,n,\mu,\nu}(x,y,z), \quad (1)$$

where K_0, L_0 are the angular and space sampling intervals, respectively, with $K_0L_0 < 2\pi$ for frame-based Gabor transformation [13]. In this work, $K_0L_0 = \pi$ is selected. $A^x_{m,n,\mu,\nu}$ is the frame-based Gabor transform coefficient for individual sub-GB and m, n, μ, ν represent the discrete sampling position in four-dimension phase-space lattice, where $-M/2 \le |m|, |\mu| \le M/2$ and $-N/2 \le |n|, |\nu| \le N/2$. M, N correspond to the contributing spatial terms and spectral terms per dimension, respectively. The number of spectral terms should be power of 2 in order to employ Fast Fourier Transform (FFT) process to evaluate the coefficients $A^x_{m,n,\mu,\nu}$ [10]. In (1), $B_{m,n,\mu,\nu}$ defines a circular GB which emerges from $[x - mL_0, y - \mu L_0, 0]$ on expansion plane ($z = 0$) and propagates along $\hat{z}_i = [nK_0, \nu K_0, \sqrt{k_0^2 - (nK_0)^2 - (\nu K_0)^2}]/k_0$ direction. k_0 is the wave number in free space. The radiated GB can be written as a general GB in the form of complex ray [14]:

$$B_{m,n,\mu,\nu}(x_i,y_i,z_i) = B_0\sqrt{\frac{\mathrm{Det}\left[Q(z_i)\right]}{\mathrm{Det}\left[Q(0)\right]}}\, e^{-jk(z_i+(1/2)\eta^T Q(z_i)\eta)}, \quad (2)$$

where $\eta \equiv \begin{bmatrix} x_i \\ y_i \end{bmatrix}$ defined in the beam-related coordinate $\hat{x}_i\hat{y}_i\hat{z}_i$. $Q(z)$ is the complex phase matrix given by

$$Q(z) = \begin{bmatrix} \dfrac{1}{z+jb_1} & 0 \\ 0 & \dfrac{1}{z+jb_2} \end{bmatrix}. \quad (3)$$

b_1, b_2 are related to the beam waists of the expanded GB with $b = k_0w_0^2/2$ on two orthogonal planes. In the expansion process, b_1 b_2 are equal to each other with the same beam radius w_0:

$$w_0 = c_0L_0\sqrt{\frac{\left(1-(nK_0/k_0)^2-(\nu K_0/k_0)^2\right)}{\lambda}}, \quad \text{with } c_0 = \frac{2\pi}{K_0/L_0}. \quad (4)$$

When the sub-GBs are traced into the reflector, reflection and diffraction are then evaluated. In [15], a closed form of 3D GB incident on a curved surface is derived for both reflection and diffraction. The diffraction solution is extended in [12] to handle more general cases when the edge plane is not lying along the principal direction of the surface, making the solution capable of analyzing offset reflectors. Illustration of 3D GB incident on a curved surface is depicted in Figure 2, where $\hat{x}_i\hat{y}_i\hat{z}_i$, $\hat{x}_1\hat{y}_1\hat{z}_1$, and $\hat{x}\hat{y}\hat{z}$ are denoted as the incident, edge, and principal coordinates, respectively. The edge coordinate has a α_i rotation angle with the principal axis and the edge is lying at $\hat{x}_1 = x_e$ plane. The origins of all

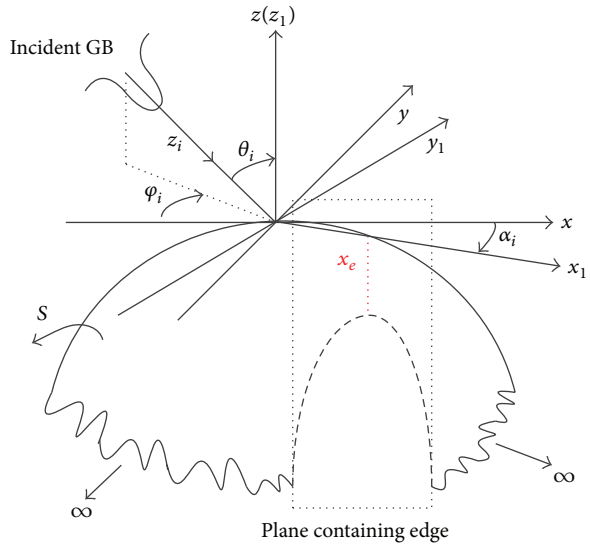

FIGURE 2: 3D GB diffraction from a semi-infinite surface containing a plane edge. $\hat{x}\hat{y}\hat{z}$ is the principal coordinate at the intersection point and the edge lies at $\hat{x} = x_e$ plane.

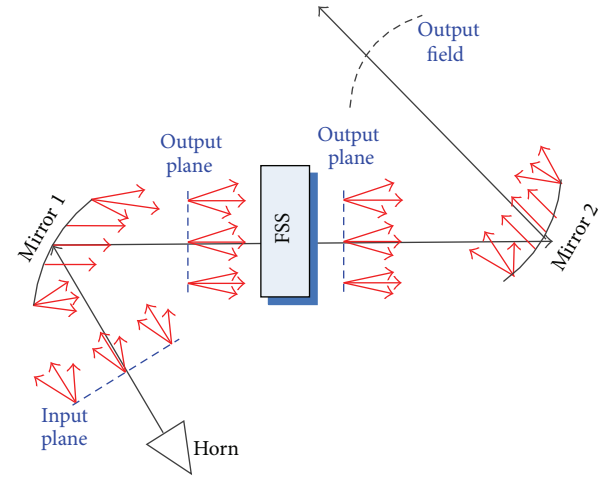

FIGURE 3: Scheme of Gaussian beam analysis of QON with FSS.

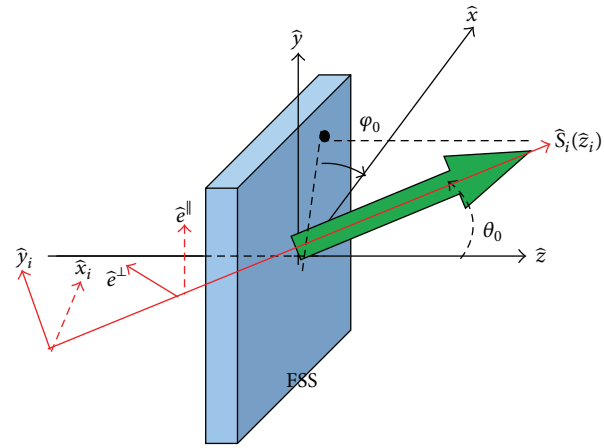

FIGURE 4: Illustration of single sub-GB passing through FSS structure.

coordinate systems coincide with each other for convenience. For reflection, the position of the edge plane goes to infinity. The analytic expression for the curved surface is given by

$$z = -\frac{1}{2}\left[\frac{x^2}{R_1} + \frac{y^2}{R_2}\right], \tag{5}$$

where R_1 and R_2 are the curvature radii in principal coordinates.

Based on Fresnel approximation of current integrals over the curved surface, the scattered field in Fresnel zone can be approximated as [15]

$$\overline{H}^s(x, y, z) = \frac{-jk}{2\pi}\frac{e^{-jkr}}{r}\left[\overline{W}_{00}I_{00}^d + \overline{W}_{10}I_{10}^d + \overline{W}_{01}I_{01}^d\right]. \tag{6}$$

$\overline{W}_{00}, \overline{W}_{01}, \overline{W}_{10}$ and $I_{00}^d, I_{10}^d, I_{01}^d$ could be found in [15]. Equation (6) is the general expression involving both reflection and diffraction. As for reflection, if the spot size of an incident GB on the surface, defined as the diameter at which the beam intensity has fallen to $1/e^2$, is much smaller than the curvature radii of the surface, the reflected field could be approximated as another GB; otherwise, the general formula should be used. The coordinate transformation is employed to extend the diffraction solution to practical cases and the detailed procedure is given in [12]. Importantly, the Gaussian beam method proposed in [12] has been extended to analyze the quasi-optical system containing FSS components. A QON system including a feed horn, a FSS, and two reflectors is depicted in Figure 3.

To analyze the FSS, one may expand the input field in front of the FSS into angular spectrum components via plane wave expansion, as shown in [11]. Reflected or transmitted spectrum components are computed by multiplying the coefficients with the corresponding plane wave. The reflected or transmitted spectrum distribution can be calculated by superposing all the plane wave components and the reflected or transmitted field on the output plane is obtained via an inversed FFT process on the spectrum distribution. In practice, the beam waists of the expanded sub-GB are in the order of several wavelengths, which is much larger than the dimension of the unit cell of the FSS. Therefore, the expanded sub-GB can be locally considered as a plane wave. Alternatively, the sub-GB coefficients are directly weighted by the reflection and transmission coefficients of the FSS and the field on the output plane can then be calculated by superposing all the reflected or transmitted sub-GBs, without the need of inversed FFT process. In addition, the attraction of the sub-GBs technique is that the number of beams needed to trace could be reduced in contrast to the number of rays in plane wave expansion [16, 17], which could improve the algorithm efficiency.

A single sub-GB passing through a FSS structure is shown in Figure 4, where $\hat{x}\hat{y}\hat{z}$ is the FSS coordinate with $\hat{z}$ normal to

the surface and $\hat{s}_i$ is the direction of the sub-GB with incident angles of $\{\theta_0, \varphi_0\}$. The incident sub-GB is given by

$$\begin{aligned}\overline{H^i}(x_i, y_i, z_i) &= \left[\hat{x}_i A^x_{m,n,\mu,\nu} + \hat{y}_i A^y_{m,n,\mu,\nu}\right] B(x_i, y_i, z_i) \\ &= \bar{e}_i B(x_i, y_i, z_i).\end{aligned} \tag{7}$$

$A^x_{m,n,\mu,\nu}$ and $A^y_{m,n,\mu,\nu}$ are the Gabor transformation coefficients along the $\hat{x}_i$ $\hat{y}_i$, respectively.

The vertical (TE) and horizontal (TM) directions of incident plane wave component are defined by

$$\begin{aligned}\hat{e}^{\perp} &= \frac{\hat{s}_i \times \hat{z}}{\left\|\hat{s}_i \times \hat{z}\right\|}, \\ \hat{e}^{\parallel} &= \hat{e}^{\perp} \times \hat{s}_i.\end{aligned} \tag{8}$$

Thus, the expansion coefficients can be projected onto the vertical and horizontal directions:

$$\begin{aligned}E^i_{nV} &= \bar{e}_i \cdot \hat{e}^{\perp}, \\ E^i_{nH} &= \bar{e}_i \cdot \hat{e}^{\parallel}.\end{aligned} \tag{9}$$

Writing in a transmission matrix way, the vertical and horizontal components for the transmitted sub-GB can be written as

$$\begin{bmatrix} E^t_{nV} \\ E^t_{nH} \end{bmatrix} = \begin{bmatrix} T_{11} & T_{12} \\ T_{21} & T_{22} \end{bmatrix} \begin{bmatrix} E^i_{nV} \\ E^i_{nH} \end{bmatrix}. \tag{10}$$

T_{11}, T_{12}, T_{21}, and T_{22} are the transmission coefficients of a TE wave into a TE wave, a TM wave into a TE wave, a TE wave into a TM wave, and a TM wave into a TM wave, respectively. Similarly, the vertical and horizontal polarization components of the reflected sub-GB are calculated by

$$\begin{bmatrix} E^r_{nV} \\ E^r_{nH} \end{bmatrix} = \begin{bmatrix} R_{11} & R_{12} \\ R_{21} & R_{22} \end{bmatrix} \begin{bmatrix} E^i_{nV} \\ E^i_{nH} \end{bmatrix}. \tag{11}$$

R_{11}, R_{12}, R_{21}, and R_{22} are the reflection coefficients. The TE and TM transmission and reflection coefficients of the FSS, which might be computed numerically via PMM method [11] or calculated in CST microwave studio software, are stored in a tabulated form. Since the sub-GBs may propagate along any direction (related to angular spectra n and ν), interpolation can be performed to compute the coefficients for the given angle of incidence $\{\theta_0, \varphi_0\}$. Once the horizontal and vertical polarization components of the sub-GB are obtained, the transmitted or reflected output field can be calculated via superposition of all the sub-GBs. At this phase, frame-based Gabor transformation can be employed again to expand the output field into a series of sub-GBs and these beams are then traced to the next reflector, which makes the analysis procedure highly modular.

In summary, the simulation process of the overall system is as follows:

(a) In analysis of Mirror 1, the field radiated from the horn on the input plane is expanded into a set of sub-GBs via frame-based Gabor transformation and then these individual GBs are traced into the reflector. The analytic expressions of reflection or diffraction of a GB incident on the reflector developed in [12] are utilized to compute the field on the output plane, which is chosen in front of the FSS along the beam propagation direction.

(b) To include the FSS, the output field of Mirror 1 servers as the input field of the FSS. Therefore, frame-based Gabor transformation is employed again to compute the coefficients of the sub-GBs. The reflected or transmitted sub-GB coefficients are directly weighted by the reflection or transmission coefficients of the FSS, depending on the system design. For instance, the transmitted field on output plane after the FSS in Figure 3 is calculated via summation of all the sub-GBs.

(c) To compute the output field of Mirror 2, the field on output plane given by step 2 is used as the input field. At this phase, analysis of the output field for Mirror 2 is quite similar to the process of Mirror 1.

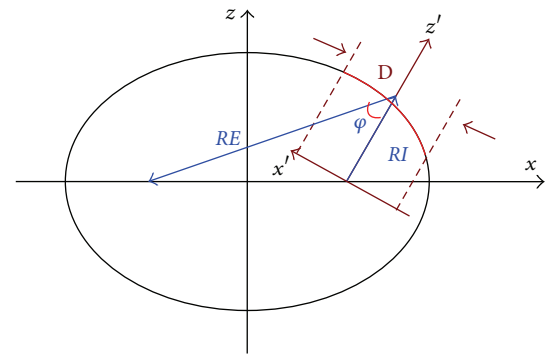

Figure 5: Illustration of ellipsoidal reflector.

3. System Design

3.1. Design of Optical Layout. The layout design of the QON system is to use a series of quasi-optical components to transform the GB radiated from the feed horn to a desired one in a limited space. Ellipsoidal reflectors are often used for beam forming in the QON system. The geometrical structure of the ellipsoidal surface is depicted in Figure 5 where RI and RE are the distances from the foci. The subtended angle by the incident and outgoing rays is φ. The ellipsoidal reflector can be regarded as a thin lens with effective focus length as f:

$$\frac{1}{f} = \frac{1}{RI} + \frac{1}{RE}. \tag{12}$$

The phase error across the surface can be avoided if the input beam has the radius of curvature $R_{\text{in}} = RI$ and the output beam has the radius of curvature $R_{\text{out}} = RE$ [18]. The diameter of reflector is D which is selected larger than twice of the spot size of the beam on the surface to avoid significant energy loss.

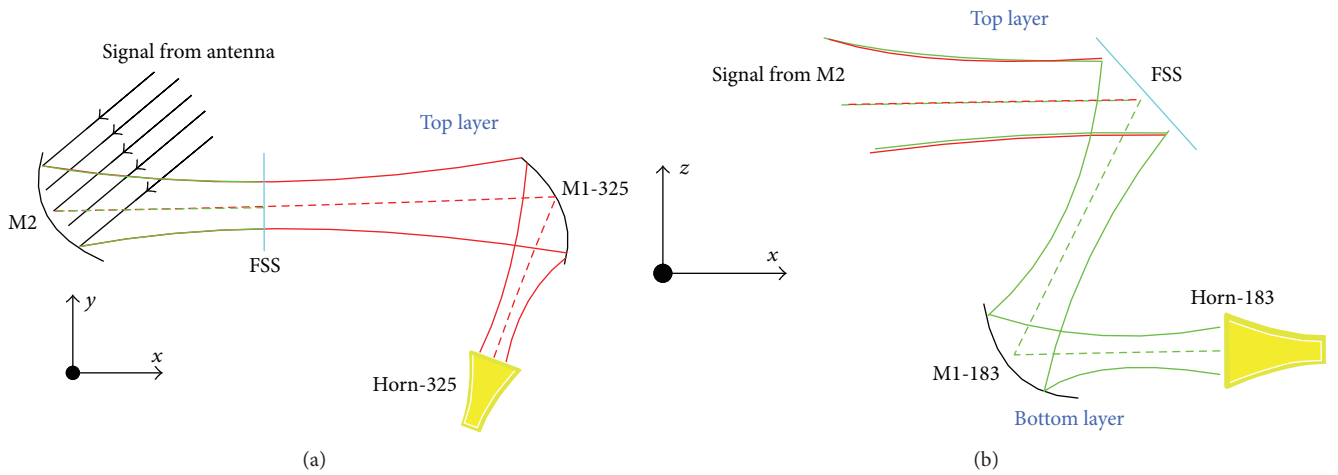

Figure 6: System layout of the 3D QON system: (a) top view of 325 GHz channel; (b) side view of 183 GHz channel.

The first consideration for system layout design is the beam incident angle. When the fundamental GB mode is incident upon an offset reflector, most of the energy reflected from the surface remains in the fundamental GB mode. However, a few higher modes are generated introducing an amplitude distortion, which is related to the incident angle. The distortion parameter U is defined as [18]

$$U = \frac{\omega_m \tan\theta_i}{2\sqrt{2}f}, \tag{13}$$

where ω_m is the beam radius at the mirror while θ_i is the incident angle. It is seen that the smaller the incident angle, the less the distortion. Nevertheless, a small incident angle may bring blockage in the QON system. Therefore, a trade-off has to be taken. In this design, an incident angle of 30 degrees is chosen as a trade-off scheme.

The second factor to be considered is frequency separation scheme. Since there are only two channels in our system, one can choose to transmit the 183 GHz signal and reflect the 325 GHz signal and vice versa, depending on the property of the FSS. The FSS in this system has better transmission performance at 325 GHz than that at 183 GHz under 30-degree incident. Therefore, the 325 GHz channel is designed to be transmitted while the 183 GHz channel is reflected.

The last but most important factor is the 3D quasi-optical layout design. The design of 3D quasi-optical system requires guiding the signal into 3D to make the most of the limited space. For the two-channel system, one can use planar or curved mirrors to redirect the signal, which, however, would possibly bring in more quasi-optical components and complicate the design. In this design, the FSS is utilized as the redirecting component, diverting the incident beam of 183 GHz to the perpendicular plane. A resultant two-layer structure employed for the 3D QON system is depicted in Figure 6. Both channels share the same M2 mirror to receive the signal from the antenna and the 325 GHz signal is transmitted through the FSS on the top layer while the 183 GHz signal is directed to the bottom layer.

3.2. Design of Frequency Selective Surface. In this QON system, the FSS is used as a high-pass filter, which transmits the 325 GHz signal and reflects the 183 GHz signal. The expected loss is no more than 1 dB in this system. Bandwidth is another concern particularly for 325 GHz channel. A multilayer FSS provides an increased bandwidth while it increases the manufacture cost as well. Furthermore, multilayer structure brings difficulty in system manufacture at submillimeter wave band. To make a trade-off, a perforated single layer planar FSS [19] is designed and fabricated. The FSS consists of slot-type hexagon arrays and the unit element geometry; the FSS is shown in Figure 7. The parameters are $a = 0.22$ mm, $d = 0.78$ mm. The manufactured dimension of the FSS is 40 mm by 40 mm with the thickness of 0.25 mm.

The FSS is simulated and optimized in CST microwave studio software. The material of FSS is set to be steel and the incident angle is chosen to be 30 degrees. The simulated and measured performance of FSS are demonstrated in Figure 8. In the picture, the black dotted line is the simulated reflection characteristics while the blue dashed line and red solid line correspond to the simulated and measured transmission loss, respectively. The measurement is only carried out for the transmission characteristics from 220 GHz to 340 GHz due to lack of instruments. It can be seen that there is a 30 dB transmitted loss at 183 GHz in the simulation, indicating a small reflection loss in this channel. Good agreement can be found between the simulated and measured transmission results in the measured frequencies. The insertion loss at 325 GHz is our major concern and is required to be less than 1 dB in the system. An insertion loss of 0.56 dB can be observed for simulation while it is 0.67 dB in the measurement at 325 GHz, which satisfies the system requirement. The bandwidth of FSS at 325 GHz can achieve about 4 GHz (from 322 GHz to 326 GHz) within the 1 dB insertion loss, which is satisfactory in this design.

3.3. Design of Corrugated Horn. Corrugated horns are often utilized in the QON system to provide axially symmetric

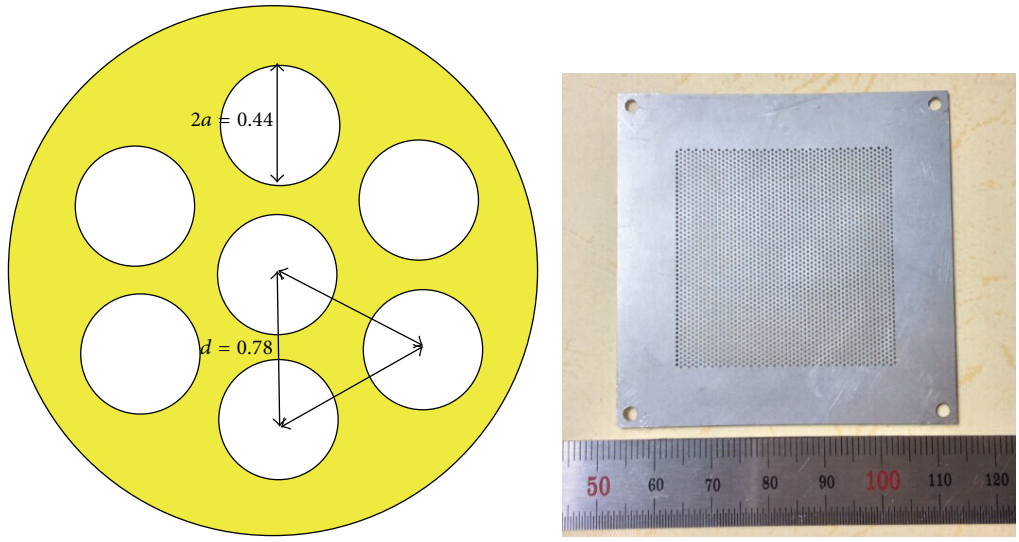

(a) (b)

Figure 7: Designed and fabricated FSS: (a) unit element geometry; (b) manufactured prototype.

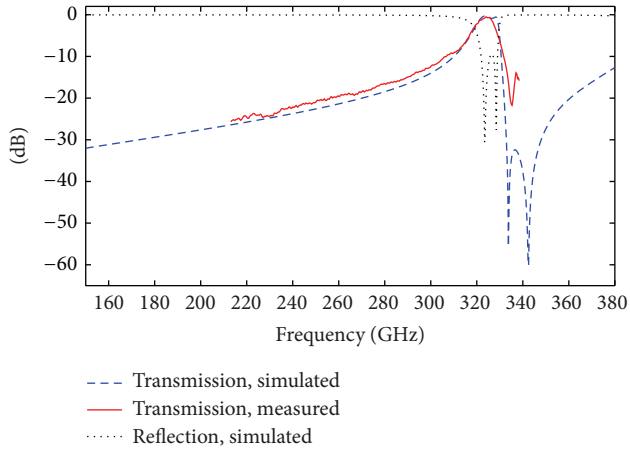

Figure 8: Transmission and reflection performance of proposed FSS.

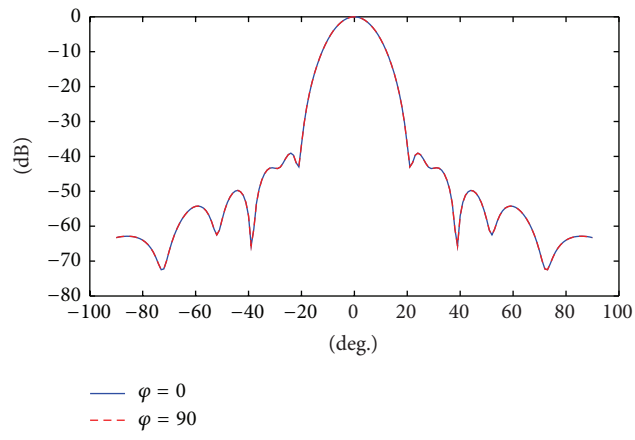

(a)

(b)

Figure 9: 183 GHz corrugated horn: (a) predicted far field pattern; (b) fabricated prototype.

radiation pattern over a wide spectral bandwidth. The radiation pattern of the feed is required to be like a fundamental Gaussian beam as much as possible. Traditionally, the horns are designed to couple TE_{10} mode from rectangular waveguide into HE_{11} mode on the aperture which has about 98% efficiency to the fundamental Gaussian mode. However, in [20], HE_{12} mode is deliberately added into HE_{11} mode and brought in phase on the aperture via a straight section of the corrugated guide, which improves the purity of fundamental Gaussian mode to be 99.8%. The design methodology is utilized in this work to design two corrugated horns with center frequency of 183 GHz and 325 GHz, respectively. The predicted far field patterns and prototypes of the corrugated horns are shown in Figures 9 and 10. The 183 GHz feed horn is designed to have −16 dB taper at the angle of 15 degrees while the 325 GHz feed horn has −15 dB taper at 15 degrees. It can be seen that both patterns exhibit Gaussian shape and the side lobe level is down to −40 dB. The feed horns are electroforming and gold-coating.

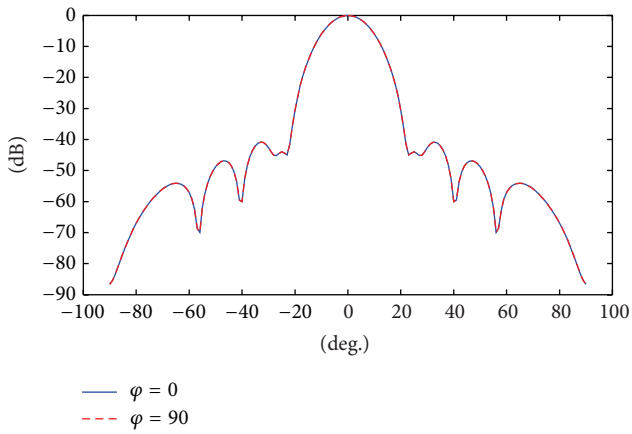

(a)

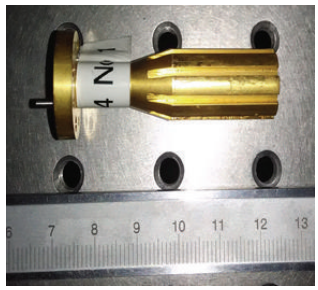

(b)

FIGURE 10: 325 GHz corrugated horn: (a) predicted far field pattern; (b) fabricated prototype.

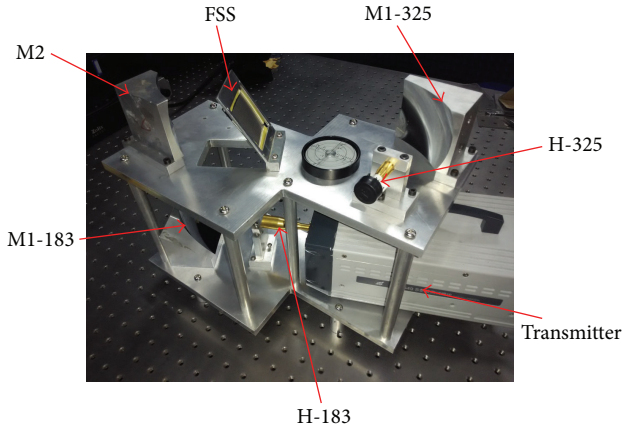

FIGURE 11: Prototype of 3D quasi-optical system.

4. Manufacture and Testing

Figure 11 shows a photograph of the two-channel 3D Quasi-Optical Test Bench fixed in a space of 330 mm by 220 mm by 229 mm. As shown in Figure 11, the lateral space is greatly saved. The height of the system is intentionally enlarged for testing convenience, which, however, can be further optimized. H-183 and H-325 are the two corrugated horns used to generate the desired Gaussian beams as the sources in measurement. M1-183, M1-325, and M2 are three ellipsoidal reflectors used to transform the Gaussian beams from the feed horns. The RMS surface tolerance of the mirrors is less than 5 microns, which meets the surface accuracy requirement at 325 GHz. During the measurement, the 325 GHz signal generated from corrugated horn H-325 is reflected by M1-325 mirror and transmitted through the FSS into the M2 reflector on the top layer. The 183 GHz channel is a little complicated where the radiated signal from H-183 is reflected from M1-183 reflector on the bottom layer and passes through the rectangular hole into the FSS on the top layer. The FSS then reflects the 183 GHz signal into the M2 mirror. As shown in the picture, the FSS combines both channels' signal to share the same reflector M2. The 183 GHz and 325 GHz signals are produced by submillimeter frequency multipliers from a 26.5 GHz millimeter wave vector network analyzer. Both feed horns are operating in vertical polarization.

The analysis of the QON has been conducted by using the aforementioned algorithm. Near field measurement is performed to verify the system design. The measured plane is chosen 150 mm in front of the M2 mirror. Both the 183 GHz and 325 GHz channels are only measured for the copolarized component at their center frequencies. The dimension of the scanning plane for 183 GHz is 96 mm by 96 mm while it is 66 mm by 66 mm for 325 GHz path. Measured near field amplitude and phase distributions of 183 GHz and 325 GHz are shown in Figures 12 and 13, respectively. The beam coupling coefficients [21], defined as the integral of the complex conjugate of the ideal Gaussian beam E_{ideal} and the measured beam E_{mea}, as represented by (14), are found to be 97.24% and 98.88% for 183 GHz channel and 325 GHz channel, respectively. The electric field distribution of the ideal Gaussian beam is a circular GB and can be calculated via the ABCD matrix describing a Gaussian beam propagation from the feed to the measured plane. Consider

$$c = \int\int E^{*}_{\text{ideal}} E_{\text{mea}}\, dx\, dy. \tag{14}$$

Figures 14 and 15 present the calculated and simulated far field results and the field difference at 183 GHz on two orthogonal cuts. The calculated far field results are obtained via performing a FFT process on the measured near field data. It can be seen that there are some deviations between the calculated and simulated far field patterns below −30 dB, which is, however, less significant in practical applications. On the vertical cut, a ±1.25 dB filed deviation can be observed within 15 degrees, corresponding to −30 dB field level while a slightly larger difference on the horizontal cut is observed. Comparisons between the calculated and simulated far field results of the 325 GHz channel are depicted in Figures 16 and 17. From the results, the agreements in the main beam are good within 10 degrees of the radiation patterns, which is also corresponding to −30 dB field level. The field differences are also demonstrated, showing ±2 dB deviations on horizontal cut and ±1 dB for the vertical plane. It can be concluded that the deviations on the horizontal planes are slightly larger than that on the vertical planes for both channels. This can be attributed to the assembly error of the system on the asymmetrical plane. Furthermore, manufactured surface accuracy of the FSS is very critical at such high frequency and a minor

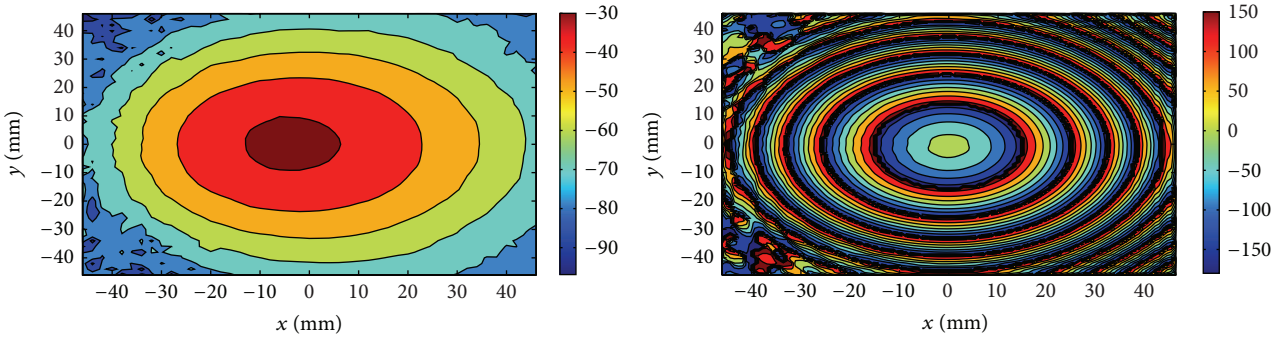

Figure 12: Measured near field amplitude and phase distributions of 183 GHz channel.

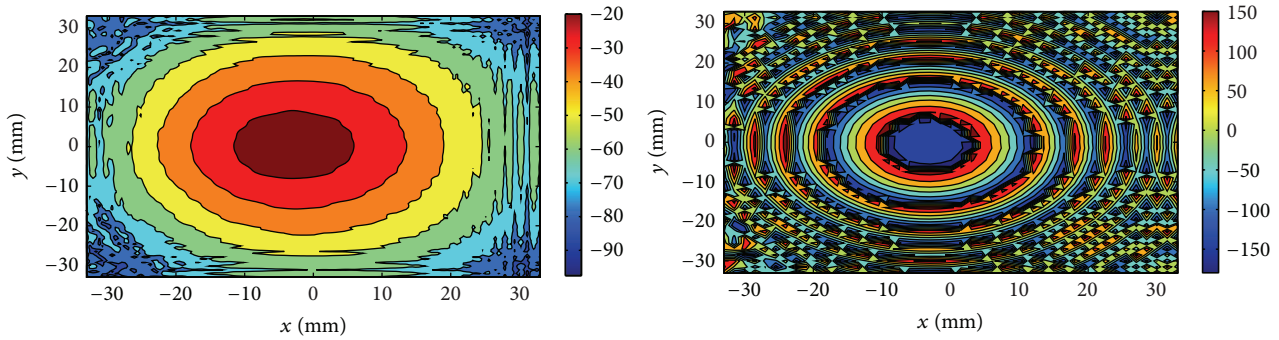

Figure 13: Measured near field amplitude and phase distributions of 325 GHz channel.

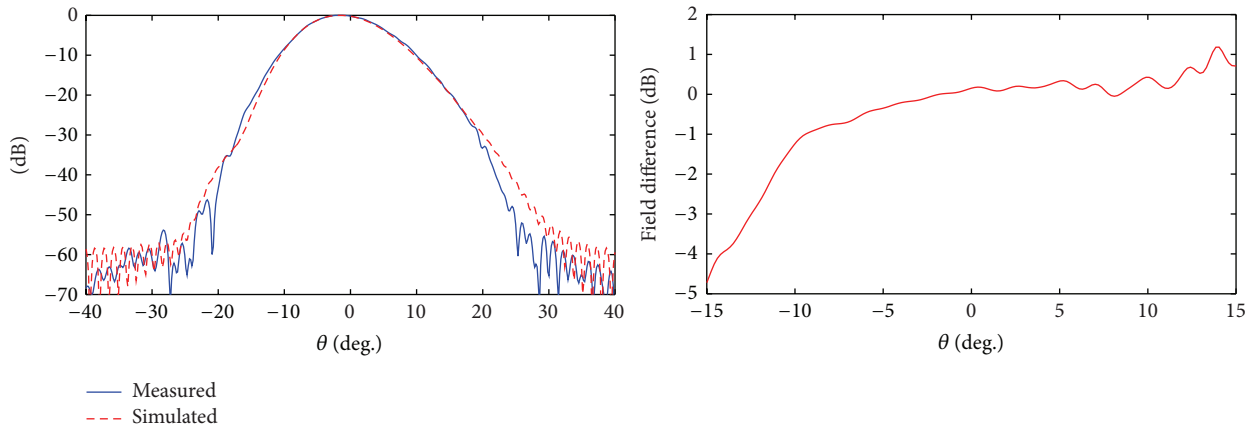

Figure 14: Calculated and simulated far field patterns of the 183 GHz channel on horizontal plane.

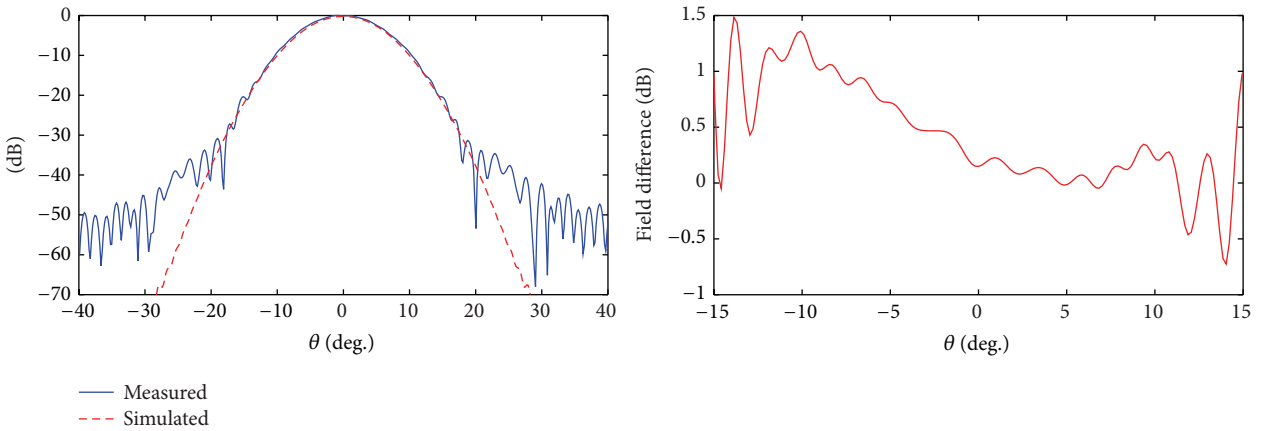

Figure 15: Calculated and simulated far field patterns of the 183 GHz channel on vertical plane.

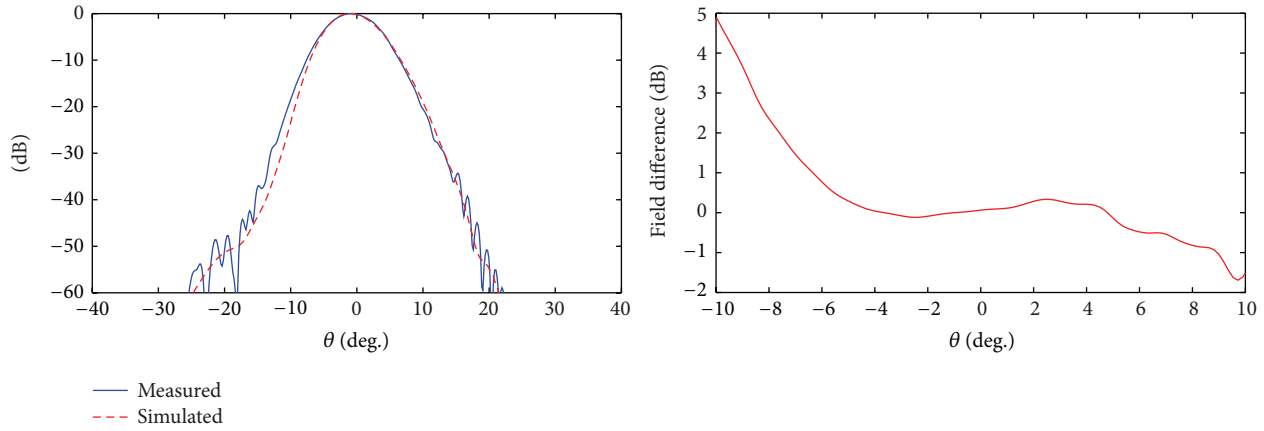

Figure 16: Calculated and simulated far field patterns of the 325 GHz channel on horizontal plane.

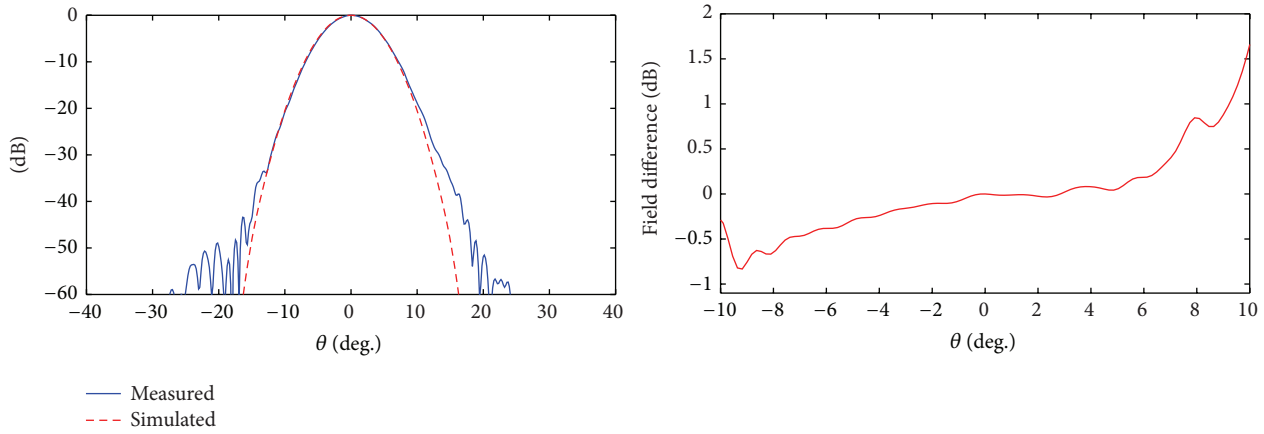

Figure 17: Calculated and simulated far field patterns of the 325 GHz channel on vertical plane.

distortion might result in a small field deviation. However, the agreements between simulations and measurements are still on a reasonable level for prototype verifications.

5. Conclusion

A 3D dual-channel QO system operating at 183 GHz and 325 GHz is designed, fabricated, and measured in this paper, in order to validate a modular Gaussian beam method for electrically large 3D QON system. The QO system has a two-layer structure, which is size-economical and makes the overall enclosure compact. The slot-type FSS with hexagonal lattice transmits the 325 GHz signal on the top layer while it redirects the 183 GHz signal into the bottom layer. Simulated and measured transmission characteristic of the FSS are presented and the insertion loss is less than 0.7 dB at 325 GHz, meeting the system requirement. Two hybrid modes' corrugated horns are also designed and fabricated to serve as the feeds. Measured results conducted via near field probing demonstrate a good agreement down below −30 dB with predicted ones within the main beam of the far field pattern. Therefore, the proposed method can be utilized to analyze the full 3D QON system as a whole.

Conflict of Interests

The authors declare that they do not have any commercial or associative interest that represents a conflict of interests in connection with the work submitted.

Acknowledgments

This work was supported in part by National Natural Science Foundation of China (no. 61201026 and no. 61401031), Beijing Higher Education Young Elite Teacher Project (no. YETP0438), the Scientific Research Foundation for the Returned Overseas Chinese Scholars, and Fundamental Research Fund for the Central Universities of China. The authors thank CST company for providing free license.

References

[1] R. J. Martin and D. H. Martin, "Quasi-optical antennas for radiometric remote-sensing," *Electronics and Communication Engineering Journal*, vol. 8, no. 1, article 37, 1996.

[2] R. Jørgensen, G. Padovan, P. de Maagt, D. Lamarre, and L. Costes, "A 5-frequency millimeter wave antenna for a

spaceborne limb sounding instrument," *IEEE Transactions on Antennas and Propagation*, vol. 49, no. 5, pp. 703–714, 2001.

[3] M. Oldfield, B. P. Moyna, E. Allouis et al., "MARSCHALS: development of an airborne millimeter-wave limb sounder," in *Sensors, Systems, and Next-Generation Satellites V*, vol. 4540 of *Proceedings of SPIE*, pp. 221–228, Toulouse, France, September 2001.

[4] D. Doyle, G. Pilbratt, and J. Tauber, "The herschel and planck space telescopes," *Proceedings of the IEEE*, vol. 97, no. 8, pp. 1403–1411, 2009.

[5] M. Griffin, B. Swinyard, L. Vigroux et al., "Herschel-SPIRE: design, ground test results, and predicted performance," in *Space Telescopes and Instrumentation: Optical, Infrared, and Millimeter*, vol. 7010 of *Proceedings of SPIE*, p. 12, Marseille, France, July 2008.

[6] P. F. Goldsmith and D. C. Lis, "Early science results from the heterodyne instrument for the far infrared (HIFI) on the herschel space observatory," *IEEE Transactions on Terahertz Science and Technology*, vol. 2, no. 4, pp. 383–392, 2012.

[7] M. Candotti, A. M. Baryshev, and N. Trappe, "Quasi-optical assessment of the ALMA band 9 front-end," *Infrared Physics & Technology*, vol. 52, no. 5, pp. 174–179, 2009.

[8] A. Gonzalez, Y. Uzawa, Y. Fujii, and K. Kaneko, "ALMA Band 10 tertiary optics," *Infrared Physics & Technology*, vol. 54, no. 6, pp. 488–496, 2011.

[9] Y. Zhang, J. Miao, H. Zhao, G. Cui, and Y. Shi, "A five-frequency bands quasi-optical multiplexer for geostationary orbit microwave radiometer," in *Proceedings of the 32nd IEEE International Geoscience and Remote Sensing Symposium (IGARSS '12)*, pp. 4676–4679, Munich, Germany, July 2012.

[10] C. Rieckmann, M. R. Rayner, C. G. Parini, D. H. Martin, and R. S. Donnan, "Novel modular approach based on Gaussian beam diffraction for analysing quasi-optical multi-reflector antennas," *IEE Proceedings—Microwaves, Antennas and Propagation*, vol. 149, no. 3, pp. 160–167, 2002.

[11] J. Yu, S. Liu, L. Xu et al., "An integrated quasi-optical analysis method and its experimental verification," *Journal of Infrared, Millimeter, and Terahertz Waves*, vol. 31, no. 2, pp. 181–195, 2010.

[12] Z. Lu, X. Liu, H. Wang et al., "A modular Gaussian beam analysis method based on 3D diffraction technique," *IEEE Antennas and Wireless Propagation Letters*, vol. 14, pp. 362–365, 2015.

[13] D. Lugara and C. Letrou, "Alternative to Gabor's representation of plane aperture radiation," *Electronics Letters*, vol. 34, no. 24, pp. 2286–2287, 1998.

[14] G. A. Deschamps, "Ray techniques in electromagnetics," *Proceedings of the IEEE*, vol. 60, no. 9, pp. 1022–1035, 1972.

[15] G. C. Zogbi, *Reflection and diffraction of general astigmatic Gaussian beam from curved surfacces and edges [Ph.D. thesis]*, Ohio State University, Columbus, Ohio, USA, 1994.

[16] I. Ghannoum, C. Letrou, and G. Beauquet, "A gaussian beam shooting algorithm for radar propagation simulations," in *Proceedings of the International Radar Conference 'Surveillance for a Safer World' (RADAR '09)*, Bordeaux, France, December 2009.

[17] R. Tahri, D. Fournier, S. Collonge, G. Zaharia, and G. El Zein, "Efficient and fast Gaussian beam-tracking approach for indoor-propagation modeling," *Microwave and Optical Technology Letters*, vol. 45, no. 5, pp. 378–381, 2005.

[18] P. F. Goldsmith, "Quasioptical systems," in *Practical Aspects of Quasioptical Focusing Elements*, pp. 109–115, Wiley-IEEE Press, Hoboken, NJ, USA, 1998.

[19] C.-C. Chen, "Transmission of microwave through perforated flat plates of finite thickness," *IEEE Transactions on Microwave Theory and Techniques*, vol. 21, no. 1, pp. 1–6, 1973.

[20] P. A. S. Cruickshank, D. R. Bolton, D. A. Robertson, R. J. Wylde, and G. M. Smith, "Reducing standing waves in Quasi-optical systems by optimal feedhorn design," in *Proceedings of the Joint 32nd International Conference on Infrared and Millimeter Waves and the 15th International Conference on Terahertz Electronics (IRMMW-THz '07)*, pp. 941–942, Cardiff, UK, 2007.

[21] P. F. Goldsmith, "Quasioptical systems," in *Gaussian Beam Coupling*, pp. 59–61, Wiley-IEEE Press, Hoboken, NJ, USA, 1998.